RESEARCH REPORTS

AN EXPERIMENTAL STUDY OF VORTEX TUBE WITH DOUBLE ROW NOZZLE

HEISHICHIRO TAKAHAMA, SHOSUKE TANAKA,
TAMON IKEDA and HIROSHI SUZUKI

Department of Mechanical Engineering

(Received May 1, 1965)

1. Introduction

The vortex tube is a simple device which separates a flow of compressed gas into a hot and a cold stream by means of a high speed vortex type flow.

One of the authors has already reported[1] the results of measurements of the vortex flow in the vortex tube with several different sizes under several different conditions. He has also presented[2)3)4)] formulae for the profiles of tangential velocity, temperature and energy of the air flowing in the standard vortex tube under the optimum conditions. In these studies, vortex tubes of the conventional types with nozzles fixed in one row were used.

This paper reports experimental results of the vortex tube with nozzles fixed in two rows and the results are compared with the above-mentioned results of the vortex tube with nozzles fixed in one row.

Nomenclature

G_c, G_h : mass flow leaving cold-end and hot-end, respectively
G_t : total mass flow entering the system, G_c+G_h
ξ : cold air ratio, G_c/G_t
D : inside dia. of vortex chamber, $2r_w$
d_0 : diameter of cold air orifice
N : number of nozzles
d_n : diameter of nozzle opening
r : radius
z. (z') : distance from nozzle opening in direction of tube axis, ($z'=z/r_w$)
p_t, p : total and static pressure, respectively
α : flow angle
V : velocity
u, v, w: radial, tangential and axial component of velocity, respectively
T : static temperature
T_t : stagnation temperature, $T+V^2/2c_p$
t_t', $\Delta t_d'$: nondimensional stagnation temperature and dynamic temperature de-

fined by equations (11) and (12), respectively

c_p, c_v : specific heat of air at constant pressure and constant volume, respectively

κ : the ratio of specific heats, c_p/c_v

γ : specific weight of air

M : Mach number, V/V_s

V_s : velocity of sound in air

P_r : Prandtle number

i : enthalpy of air, c_pT

i_t : total enthalpy of air, c_pT_t

φ : velocity coefficient of nozzle

Ψ : ratio of mean velocity of vortex flow near tube wall in cross-section including nozzle opening to jet velocity at exit of nozzle

Subscripts

n : entrance of nozzle

h, c : hot-end and cold-end of vortex chamber, respectively

o : cold-end orifice

s : adiabatic isentropic change

2. Experimental Apparatus and Procedure

Fig. 1 shows the schematic view of apparatus. Compressed air is cooled to constant temperature through an after-cooler, then passes a separator in order to remove drain and dust. Then the air enters a straight tube through several tangential nozzles fixed near one end. A high velocity vortex flow is set up in the straight tube. The present study covers the range of Mach numbers from 0.5 to 1. The total mass flow rate entering the system G_t kg/s and the mass

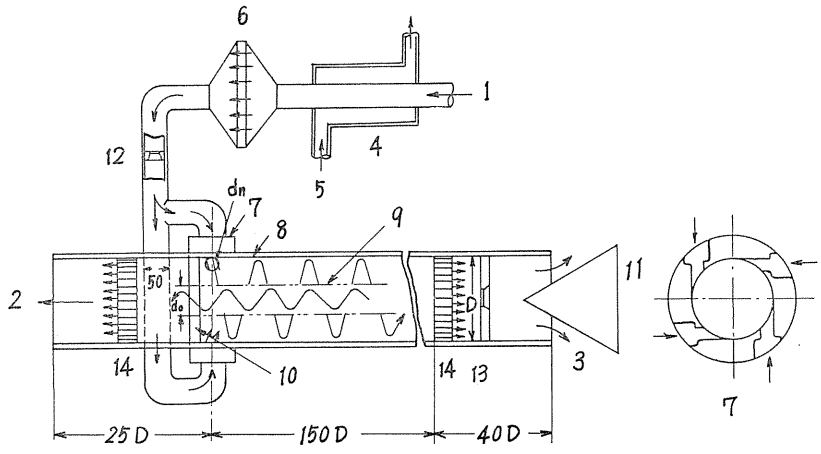

FIG. 1. Schematic diagram of test apparatus

1. Compressed air from surge tank, 2. Cold air, 3. Hot air, 4. After-cooler, 5. Cooling water, 6. Separator, 7. Nozzle, 8. Vortex chamber made of plastic, 9. Core boundary, 10. Cold-end orifice, 11, Regulation valve, 12, 13. Standard pipe orifice, 14. Rectifier.

flow rate leaving the hot-end G_h kg/s are measured by the standard pipe orifices. Both the hot air and the cold one have peripheral velocity components, so they are diminished by the rectifiers. ξ is the cold air ratio *i.e.* G_c/G_t. The value of ξ was changed by the cone valve at the hot-end of the tube, lying between 0.25 and 0.75 in these experiments. The tube length of the vortex chamber was made 150 times as long as the tube diameter considering the results of preparatory experiments; the tube was made of plastics and thermally insulated from atmosphere. Fig. 2 shows the double row nozzle. Table 1 shows the dimensions of the vortex chambers used. For each chamber with several different cold-end orifices, the performance as an energy separator was examined. A cylinder type Pitot tube with a stagnation temperature probe, the outside diameter of which is 3 mm, was used to measure the flow angle $\alpha°$, the total pressure p_t kg/m², the static pressure p kg/m² and the stagnation temperature T_t°K of the air flowing in the vortex chamber. These measurements were made in a few cross-sections of the tube. These values in the cross-section including the nozzle center were measured by a Pitot tube with stagnation temperature probe inserted axially through the cold-end orifice. The static temperature T°K, the velocity V m/s, the tangential velocity v m/s and the axial velocity w m/s of the air flow were calculated by

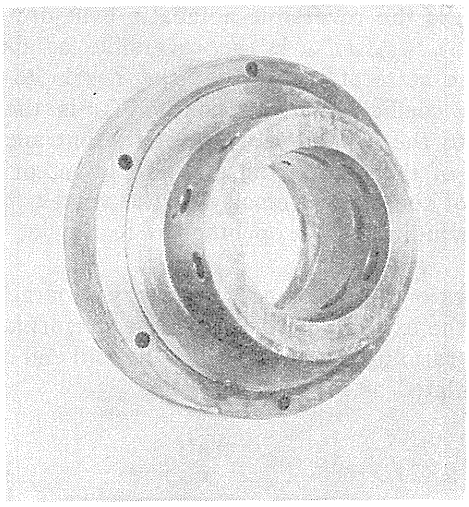

FIG. 2. Double row nozzle

TABLE 1

Test No.	Inner Dia. of Tube D_{mm} (inch)	Nozzle			d_n/D	$N(d_n/D)^2$	Optimum Dia. of cold end orifice d_0(mm)	φ***	Ψ****
		Dia. d_n (mm)	Number N	Row					
1	52.8 (2)	6.02	12	2*	0.114	0.156	23.0	0.755	1.00
2	52.8 (2)	10.91	4	1**	0.207	0.171	26.5	0.840	0.98

* Double row nozzle

** Single row nozzle *i.e.* Conventional nozzle

*** Velocity coefficient of nozzle

**** Ratio of mean velocity of vortex flow near tube wall in cross-section including nozzle opening to jet velocity at exit of nozzle

the following equations:

$$p_t/p = \{1 + (\kappa - 1)M^2/2\}^{\kappa/(\kappa-1)} \quad (1)$$

$$T_t/T = 1 + (\kappa - 1)M^2/2 \quad (2)$$

$$V_s = \sqrt{\kappa g R T} \quad (3)$$

$$V = MV_s, \quad v = V\cos\alpha, \quad w = V\sin\alpha \quad (4)$$

where M is Mach number, V_s is sound velocity m/s, κ is the ratio of specific heats of air c_p/c_v.

3. Experimental Results and Discussion

3.1. Efficiency of energy separation

The efficiency of energy separation η_i was introduced to compare the performances of vortex tubes. It is defined as follows[2]:

$$\eta_i = (i_{tn_1} - i_{tc})/\{\Psi^2\varphi^2(\Delta i)_{ns} + (\Delta i)_{cs}\}$$
$$= (T_{tn_1} - T_{tc})/\{\Psi^2\varphi^2(\Delta T)_{ns} + (\Delta T)_{cs}\} \quad (5)$$

where $(\Delta i)_{ns} = c_p(\Delta T)_{ns}$ is the reversible adiabatic heat drop of the air expanding through the nozzle, $(\Delta i)_{cs} = c_p(\Delta T)_{cs}$ is the reversible adiabatic heat drop of the air expanding from the state at the exit of the nozzle to the atmospheric pressure, φ is the velocity coefficient of the nozzle, T_{n_1} is the atmospheric temperature which is equal to the air temperature at the entrance of the nozzle, T_{tc} is the total temperature of the air leaving of the cold-end orifice and the correction factor Ψ is the ratio of the mean velocity of the vortex flow near the tube wall in the cross-section including nozzle openings U to the jet velocity at the exit of the nozzle φV_{ns}.

Fig. 3 shows values of the efficiency of energy separation η_i versus Reynolds numbers of the jet at the exit of nozzle Re. These performance tests were carried out at various cold air ratio using several different cold-end orifices. The Reynolds number of jet is calculated as follows:

$$Re = \frac{V_n D}{\nu}$$

where V_n is the jet velocity at the exit of the nozzle, D is the inside diameter of the vortex chamber and ν is the kinematic viscosity of air. Fig. 4 shows the comparison between the efficiencies of both tubes with optimum sizes of cold-end orifice.

3.2. Velocity profile

Absolute velocity The following definitions were given as illustrated in Fig. 5. V_m is the maximum velocity in the cross-section, V is the velocity at the distance y from the tube wall, V is $V_m/2$ at $y=h$ and nondimensional quantities V' and y' are V/V_m and y/h, respectively. The profiles of V' at $z' = z/r_\omega = 1$, 10 and 29 are plotted against y' in Fig. 5, where the double row nozzles are used. These profiles coincide with each other with little difference. The value of cold air rate ξ doesn't affect the nondimensional velocity profiles as shown in Fig. 6. The same

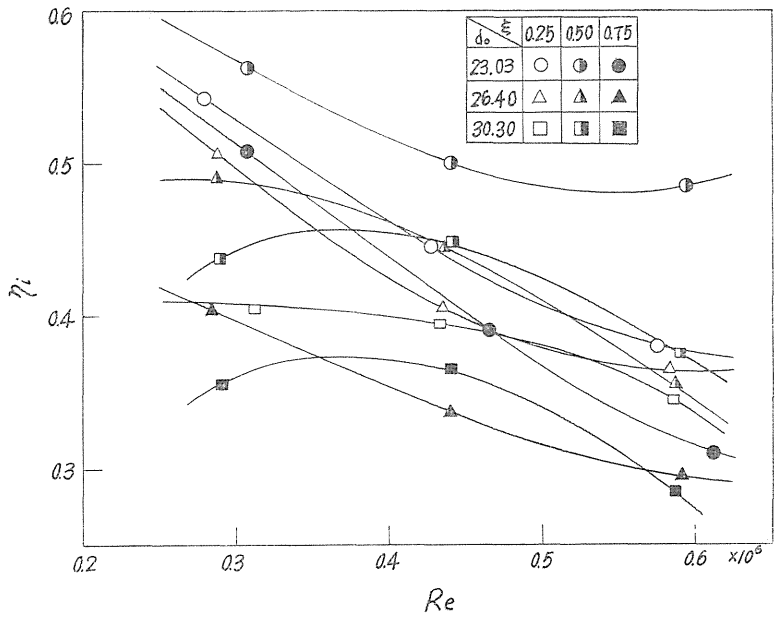

FIG. 3. Efficiency of energy separation of tube with double row nozzle versus Reynolds number at various cold air ratio using several different cold-end orifice

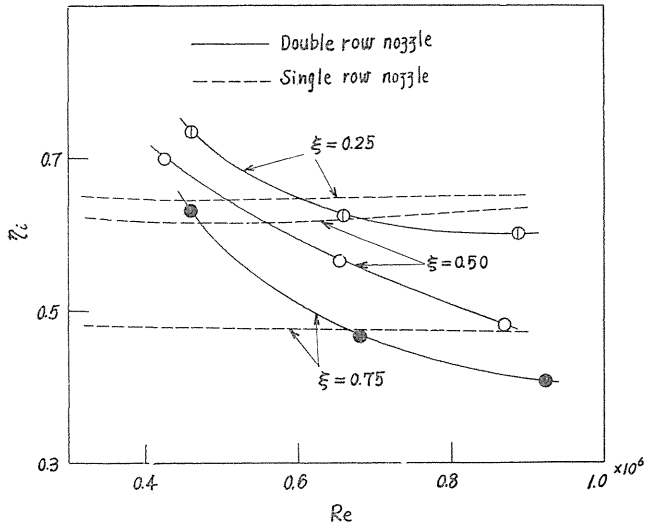

FIG. 4. Comparison between efficiency of tube with double row nozzle and that of tube with single row nozzle

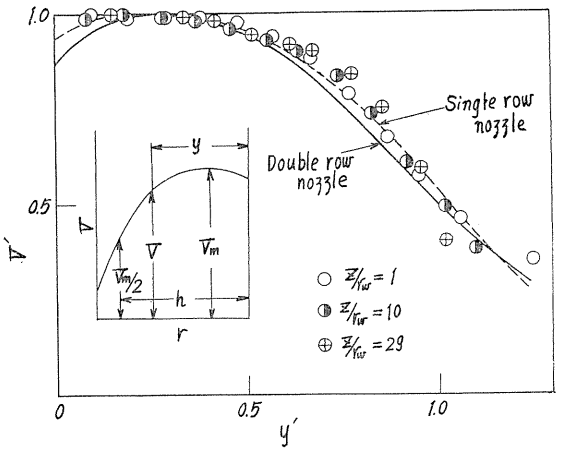

FIG. 5. Comparison of nondimensional absolute velocity distributions in different cross-sections with velocity profile computed by semi-empirical equation (6)

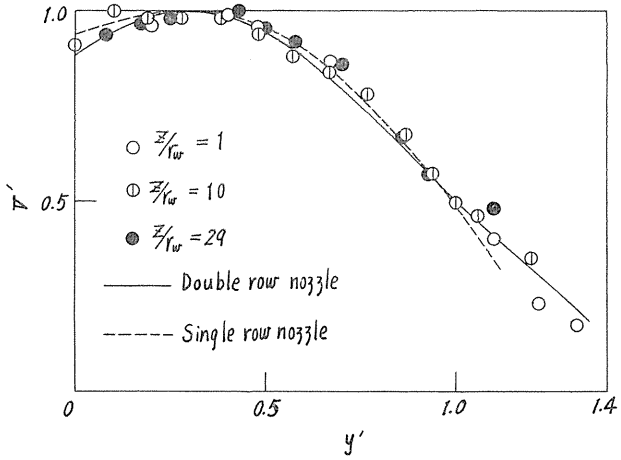

FIG. 6. Comparison of nondimensional absolute velocity distributions at different values of cold air ratio with velocity profile computed by equation (6)

results have already been reported[2)3)] for the case of vortex chamber of conventional type with a single row nozzle. The velocity profiles are computed in terms of the semi-empirical equation which has been derived in the previous report[2)].

$$V' = e^{-\lambda(y'-a)^2} \tag{6}$$

where $y'=y/h$ as mentioned bofore, $\lambda = (\log 2)/(1-a)^2$, d_n the diameter of the nozzle opening and r_w the radius of the vortex chamber. Moreover, $a=(2\,d_n/r_w)/$

$(1+2\,d_n/r_w)$ should be used for the case of double row nozzles, instead of $a=(d_n/r_w)/(1+d_n/r_w)$ for the case of single row nozzle, as will be stated in the following chapter.

Radial velocity It is assumed that the flow is axially symmetric and in steady. In this case, from the equation of continuity the radial velocity is written as follows:

$$u_{r=r_1}=\left[\frac{\partial}{\partial z}\int_0^{r_1} rw\,dr\right]\Big/ r r \tag{7}$$

Substituting the experimental values of r and w into the above equation and calculating by graphical method, there are obtained the profiles of radial velocity in the cross-section at $z'=1$ as shown in Fig. 7. There is little difference between the values of radial velocity for the double row nozzle and those for the single row nozzle, and their maximum values are less than one percent of jet velocity at the exit of the nozzle.

Usually an inward radial flow exists in every cross-section of the tube. When

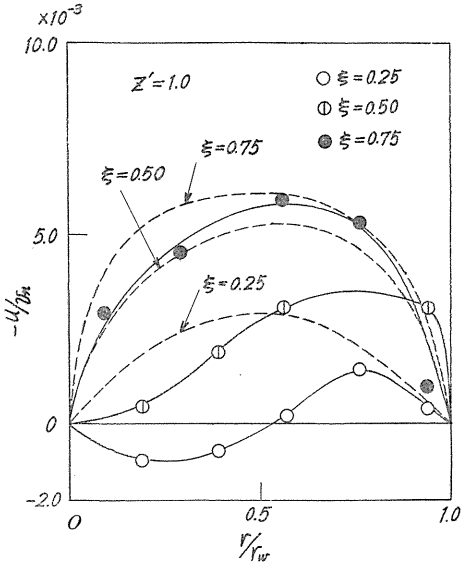

FIG. 7 (a)

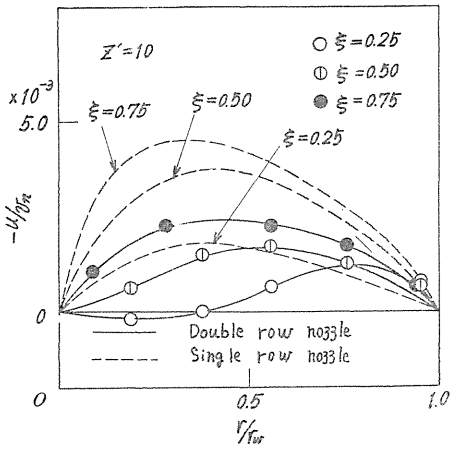

FIG. 7 (b)

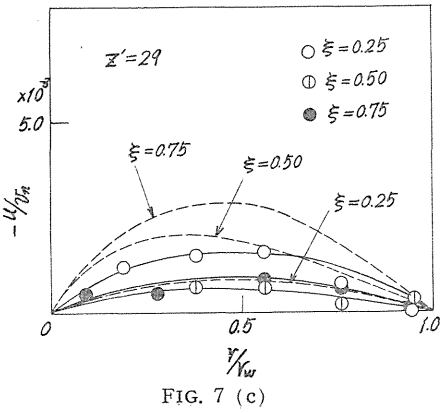

FIG. 7 (c)

FIG. 7. Radial velocity distributions in different cross-sections at different values of cold air ratio

the value of cold air ratio ξ is small in the tube with double row nozzle ($\xi \leqq 0.25$), one finds an outward radial flow in the core region of the cross-section at $z'=1$ near the nozzles, as shown in Fig. 7. It may be considered that in such a case a part of the air flowing back in the core region turns its course outward and then it flows towards the hot-end again with the air which spouts out of the nozzle. This recirculating air may be considered to prevent heat transfer from the air flowing back in the central core region to the one flowing in the annular region. Such a phenomenon decreases the performance of energy separation as shown in Fig. 4.

Back flow region i.e. Core region Fig. 8 shows the non-dimensional radii of the back flow towards the cold-end orifice. As the value of cold air ratio ξ increases, the radii of the backflow region *i.e.* core region decreases. In the vortex chamber with the double row nozzle, the thickness of the annular flow just behind the nozzles is twice the diameter of nozzle opening, then it may be considered that the jet flow from the nozzles in the back row is overlapped by the jet flow from the nozzles in the front row which is nearer than the former to the cold-end orifice.

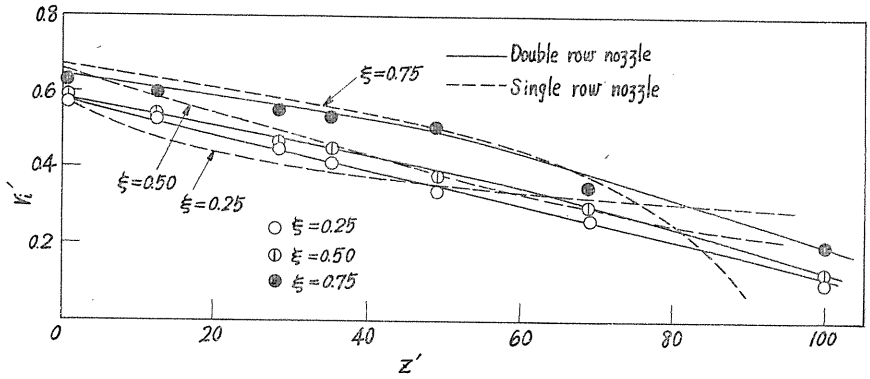

FIG. 8. Radius of back flow region

Tangential velocity Fig. 9 shows the profiles of tangential velocity in the cross-section at $z'=1$ near the nozzle openings. In the case of the single row nozzle, the range where the tangential velocity is constant is nearly equal to the diameter of the nozzle opening. But in the case of the double row nozzle, it is about twice the diameter of the nozzle opening. As mentioned before, the jet flow from the nozzles in the front row seems to overlap the jet flow from the nozzles in the back row, and the tangential velocity is constant in this annular flow. Therefore, the following equations derived in the previous reports[4] may be used to predict the profiles of tangential velocity in the cross-section near the cold-end orifice of the device with double row nozzles replacing the nozzle diameter d_n with $2d_n$;

$$r_i' \leqq r' \leqq 1\ ;\quad v' = \beta e^{-\lambda' z'} \tag{8}$$

$$0 \leqq r' \leqq r_i'\ ;\quad v' = (\beta / r_i') e^{-\lambda' z'} r' \tag{9}$$

$$\mathfrak{B} = 1 - \{N^2 d_n'^4 / 16 \Psi^2 (1 - r_i'^2)^2\} \tag{10}$$

where $v' = v/U$, $r' = r/r_w$, $z' = z/r_w$, $d_n' = d_n/r_w$, $r_i' = (r_w - d_n)/r_w$, $\Psi = U/\varphi V_{ns}$, v tangential velocity, U the mean velocity of the vortex flow near the tube wall in the cross-section including the nozzle opening, φ velocity coefficient of the nozzle and V_{ns} the velocity corresponding to the reversible adiabatic expansion through the nozzle.

In Fig. 9 the tangential velocity profile computed from the equations (8) and (9) is given by a full line.

From Fig. 9 the equations (8) and (9) may be considered the most reasonable ones for the device with the double row nozzle, except the case of smaller value of the cold air ratio ξ (*i.e.* $\xi \leqq 0.25$).

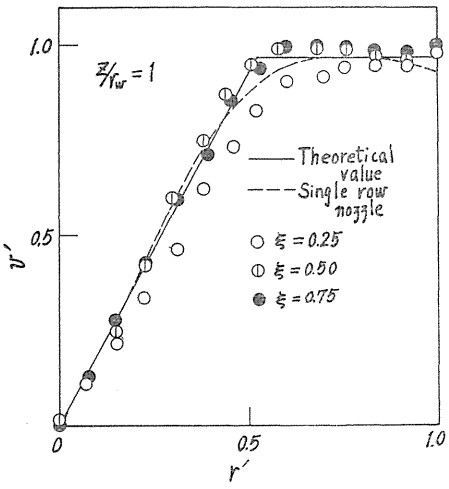

FIG. 9. Distributions of tangential velocity in cross-section at $z' = 1$

3.3. *Stagnation temperature and Dynamic temperature*

Fig. 10 shows the distribution of stagnation temperature and dynamic temperature measured in the cross-section at $z' = 1$ for the cold air ratio $\xi = 0.25$, 0.50 and 0.75. The nondimensional quantities t_t' and $\Delta t_d'$ used in Fig. 10 are defined as follows:

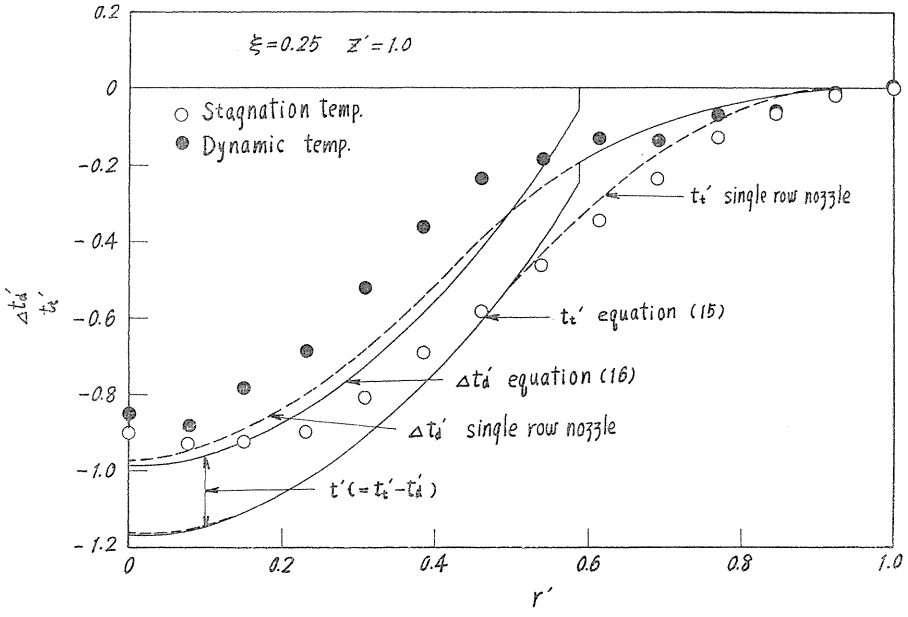

FIG. 10 (a)

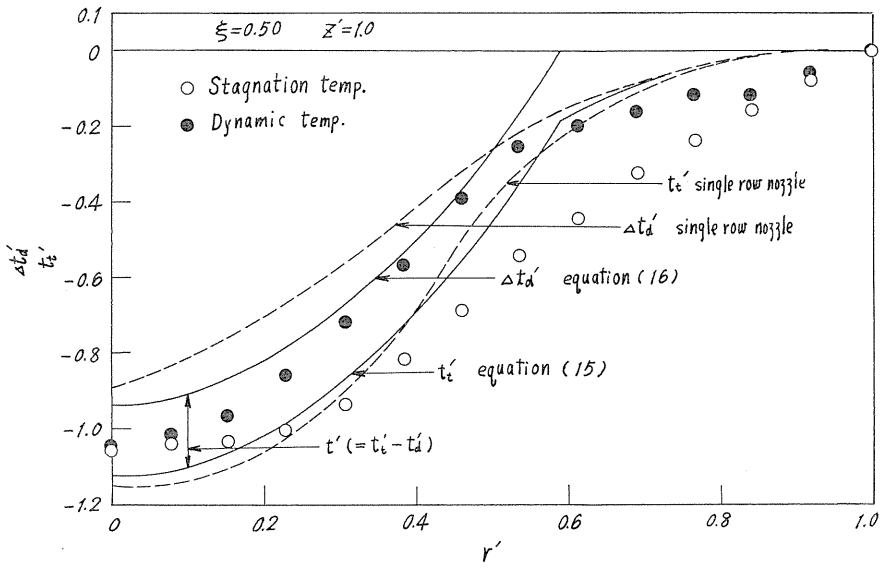

FIG. 10 (b)

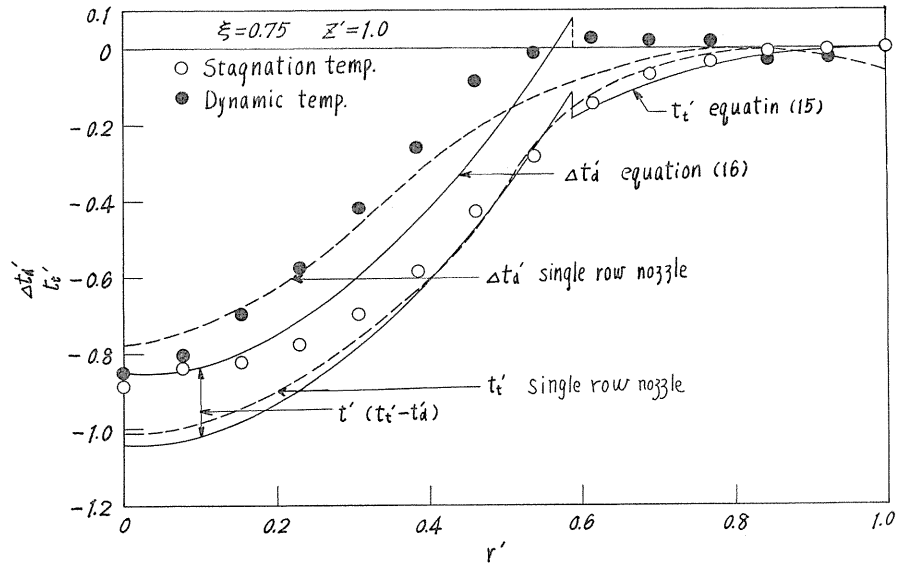

FIG. 10 (c)

FIG. 10. Comparison of experimental results with profiles of stagnation temperature and dynamic temperature computed from equations (13)-(16)

$$t'_t = (T_t - T_{tw})/(U^2/2\,c_p) \tag{11}$$

$$\Delta t'_d = (V^2/2\,c_p - V_w^2/2\,c_p)/(U^2/2\,c_p) \tag{12}$$

Where T_t and V are stagnation temperature and absolute velocity at any point, respectively, T_{tw} and V_w are the stagnation temperature and the absolute velocity

near the tube wall, respectively and U is the mean velocity near the tube wall in the cross-section including the nozzle opening. As shown in Fig. 10 for $\xi=0.50$ and 0.75, decrement of the stagnation temperature in the back flow region in the chamber with the double row nozzle are slightly less than that for the single row nozzle. Therefore, the efficiency of energy separation in the case of the double row nozzle is slightly lower than that in the case of the single row nozzle for $\xi=0.50$ and $\xi=0.75$ as already seen from Fig. 4. This tendency is more evident in the case of the cold air ratio $\xi=0.25$ as shown in Fig. 10 (a) and Fig. 4, because of the prevention of the heat transfer between the back flow and the annular flow by the recirculation of air as already stated in the section of radial velocity.

The full lines in Fig. 10 show the profiles of the nondimensional stagnation temperature t_t' and the nondimensional dynamic temperature $\Delta t_d'$ computed from the following equations (13)-(16), respectively.

$r_i' \leqq r' \leqq 1$

$$t_t' = -P_r \beta^2 e^{-2\lambda' z'} (\log r')^2 \tag{13}$$

$$\Delta t_d' = 0 \tag{14}$$

$0 \leqq r' \leqq r_i'$

$$t_t' = -P_r \beta^2 e^{-2\lambda' z'} (\log r_i')^2 + (\beta / r_i')^2 e^{-2\lambda' z'} r'^2 + [\xi N d_n'^2 / 4\Psi r_i'^2]^2 - \beta^2 e^{-2\lambda' z'} - [N d_n'^2 / 4\Psi (1 - r_i'^2)]^2 \tag{15}$$

$$\Delta t_d' = (\beta / r_i')^2 e^{-2\lambda' z'} r'^2 + [\xi N d_n'^2 / 4\Psi r_i'^2]^2 - \beta^2 e^{-2\lambda' z'} - [N d_n'^2 / 4\Psi (1 - r_i'^2)]^2 \tag{16}$$

where P_r is Prandtle number of air. These calculations were carried out by putting $r_i' = (r_w - d_n)/r_w$ in the case of the single row nozzle and $r_i' = (r_w - 2d_n)/r_w$ in the case of the double row nozzle, respectively. The equation (13) and (15) may be used to predict the profiles of the stagnation temperature in the cross-section near the nozzle accurately, except the case for $\xi \leqq 0.25$.

4. Conclusion

1. In the vortex chamber with the double row nozzle, the thickness of the annular flow just behind the nozzles is twice the diameter of nozzle opening, then it may be considered that the jet flow out of the nozzles in the back row is overlapped by the jet flow out of the nozzles in the front row which is nearer than the former to the cold-end orifice.

2. The efficiency of energy separation of the vortex tube with the double row nozzle is lower than that of the vortex tube with the conventional nozzle, especially for the smaller value of cold air ratio ($\xi \leqq 0.25$).

3. When the value of cold air ratio ξ is small ($\xi \leqq 0.25$), a part of the air flowing back ward in the core region turns its course outward near the cold-end orifice and then it flows toward the hot-end again with the air which spouts out of the nozzles.

This recirculating air may be considered to prevent heat transfer from the air flowing back in the central core region to the one flowing in the annular region. Such a phenomenon decreases the effficiency of energy seperation.

4. Replacing the radius of back flow near the nozzles $r_i=(r_w-d_n)$ with $r_i=(r_w-2d_n)$ the equations (13)-(16) derived in the previous report[2)3)4)] may be used to predict the profiles of tangential velocity, dynamic temperature and stagnation temperature in the cross-section near the cold-end orifice of the device with double row nozzles, except the case of lower value of the cold air ratio ξ ($\xi \leqq 0.25$).

Acknowledgments

The authors due to express their thanks to Mr. A. Morooka for his cooperation through his graduation-thesis in the Heat Engine Laboratory of Nagoya University.

References

1) H. Takahama and K. Kawashima, Research Report of the Faculty of Engineering, Nagoya Univercity, **Vol. 12,** No. 2 (1960), p. 227.
2) H. Takahama, Trans. Japan Soc. Mech. Engrs, **Vol. 30,** No. 219 (1964), p. 1419 (in Japanese).
3) H. Takahama, Bulletin of Japan Soc. Mech. Engrs, **Vol. 8,** No. 31 (1965), (being in press).
4) H. Takahama and N. Soga, Trans. Japan Soc. Mech. Engrs., **Vol. 31,** No. 225 (1965), p. 787 (in Japanese).